REFERENCES

Bingham, R., D.A. Bryant, and D.S. Hall (1984). A wave model for the aurora. Geophys. Res. Lett., 11, 327-330.

Bryant, D.A., D.S. Hall, and C.P. Chaloner (1985). Energization of electrons following ion releases in the solar wind. Proc. 7th ESA Symposium on European Rocket and Balloon Programmes and Related Research, SP-229, 217-220.

Bryant, D.A., S.M. Krimigis, and G. Haerendel (1985). Outline of the Active Magnetospheric Particle Tracer Explorers (AMPTE) mission. IEEE Trans. Geosci. Remote Sensing, GE-23, 177-181.

Coates, A.J., J.A. Bowles, R.A. Gowan, B.K. Hancock, A.D. Johnstone, and S.J. Kellock (1985). AMPTE UKS Three-Dimensional Ion Experiment. IEEE Trans. Geosci. Remote Sensing, GE-23, 287-292.

Dassoulas, J., D.L. Margolies, and M.R. Peterson (1985). The AMPTE CCE Spacecraft. IEEE Trans. Geosci. Remote Sensing, GE-23, 182-191.

Haerendel, G., A. Valenzuela, O.H. Bauer, M. Ertl, H. Föppl, K. -H. Kaiser, W. Lieb, J. Loidl, F. Melzner, B. Merz, H. Neuss, P. Parriger, E. Rieger, R. Schöning, J. Stöcker, E. Wiezorrek, and E. Molina (1985). The Li/Ba Release Experiments of the Ion Release Module. IEEE TRANS. Geosci. Remote Sensing, GE-23, 253-258.

Häusler, B., F. Melzner, J. Stöcker, A. Valenzuela, O.H. Bauer, P. Parigger, K. Sigritz, R. Schöning, E. Seidenschwang, F. Eberl, K. -H. Kaiser, W. Lieb, B. Merz, U. Pagel, E. Wiezorrek, and J.P. Genzel (1985). The AMPTE IRM Spacecraft, IEEE Trans. Geosci. Remote Sensing, GE-23, 192-201.

Krimigis, S.M., G. Haerendel, R.W. McEntire, G. Paschmann, and D.A. Bryant (1982). The Active Magnetospheric Particle Tracer Explorers (AMPTE) program. EOS, Trans. Amer. Geophysic. Union, 63, 843-850.

Shah, H.M., D.S. Hall, and C.P. Chaloner (1985). The Electron Experiment on the AMPTE UKS. IEEE Trans. Geosci. Remote Sensing, GE-23, 293-300.

Ward, A.K., D.A. Bryant, T. Edwards, D.J. Parker, A. O'Hea, T.J. Patrick, P.H. Sheather, K.P. Barnsdale, and A.M. Cruise (1985). The AMPTE UKS Spacecraft. IEEE Trans. Geosci. Remote Sensing, GE-23, 202-211.

Plasma Physics and Controlled Fusion, Vol. 27, No. 12A, pp. 1379–1390, 1985
Printed in Great Britain

0741-3335/85$3.00+ .00
Institute of Physics and Pergamon Press Ltd.

PRELIMINARY ICRF RESULTS FROM JET

J Jacquinot, R Anderson, J Arbez, D Bartlett, B Beaumont[1], K Behringer, E Bertolini, G Bosia, H Brinkschulte, M Bureš, D Campbell, K Christiansen, C Christodoulopoulos, R Claesen, J Cordey, S Corti, A Costley, G Cottrell, B Denne, M Evrard[3], D Gambier[1], B Green, G Grosso[7], M Huguet, ON Jarvis, A Kaye, H Kimura[6], H Krause[4], PP Lallia, P Lomas, G Magyar, M Mansfield, K Mast, PL Mondino, P Morgan, J Plancoulaine, J O'Rourke, PH Rebut, G Sadler, F Sand, M Schmid, S Segre[2], A Sibley, M Stamp, D Summers, K Thomsen[5], A Tanga, M Valisa, T Wade, C Walker

JET Joint Undertaking,
Abingdon, Oxfordshire, OX14 3EA, England

ABSTRACT

As a first step in the JET ICRF programme, two antenna generator units have been installed at Jet and operated up to the design specification of 3 MW coupled in the Torus for 1 second. After a brief description of the system, the experimental results of wave coupling to the plasma and matching the plasma loaded antenna are discussed. The first heating results are presented concentrating on the analysis of a case where the total power to the plasma increases by a ratio of 2.5. The main results are: a peak power deposition profile generating large internal temperature relaxation (giant sawteeth), a comparison of results using antennae with different wavelength radiation patterns and the low level of impurity effects.

INTRODUCTION

Successful attempts to heat magnetically confined plasmas using waves in the ion cyclotron range of frequencies (ICRF) can be traced back as early as 1960 (Stix). The complexity of the physical processes involved in the method rapidly appeared greater than expected and triggered research broadly divided into three domains:

- The near field problem which opens the way to the understanding of antenna plasma coupling and edge effects,
- The propagation towards the intended heating region which is a key to the description of the power deposition profile,
- The damping regions normally identified by a combination of processes: ion cyclotron resonance, wave mode conversion and electron damping (TTMP or Landau damping).

Progress in these subjects has been closely associated with the development of the reliable and well diagnosed plasma offered by the tokamaks. The characteristics of propagation in the form of the fast magnetosonic wave was well identified in the ST tokamak (J Adam, 1975) where sharp toroidal resonances were first observed at the expected plasma density. The paramount importance of the role played by minority ion species in the vicinity of their fundamental resonance was recognised shortly afterwards (Vdovine, 1976; Jacquinot, 1977) and opened the way to well defined heating conditions where a small amount of either

[1] From EUR-CEA Association, Fontenay-aux-Roses, France
[2] From EUR-ENEA Association, Frascati/Roma, Italy
[3] From EUR-EB Association, Brussels, Belgium
[4] From EUR-IPP Association, Garching, Federal Republic of Germany
[5] From Risø National Laboratory, Roskilde, Denmark
[6] From JAERI, Naka-Gun, Ibaraki-Ken, Japan
[7] From EUR-CNR Association, Milan, Italy

hydrogen or He^3 is used as a catalyst to obtain large damping rates in the plasma core (TFR, Equipe TFR, 1980; PLT, Hosea, 1979). With this method, a large fraction of the RF power is channelled through the minority species which become non maxwellian with an average energy much larger than the majority species. More recently, heating at the harmonic of hydrogen resonance (PLT, Hwang, 1983) sometimes enhanced by the combined use of neutral beam injection (JFT2M, Odajima, 1984), has been added to the catalogue of efficient heating scenarios.

Heating is normally associated with impurity release and edge effects. Release of impurities with a large atomic number induces line radiation losses from the plasma core at the expense of the heating efficiency. The phenomenon can be highly non linear with RF power and plasma density; it may induce a thermal instability or radiation collapse when the radiation starts exceeding the heating power flux. The thermal collapse takes the form of a very rapid and total disruption of the plasma column. Studies performed on the TFR (Equipe TFR, 1984) and TEXTOR (Messiaen, 1984) tokamaks have shown that the use of material with low atomic number (carbon) in the antenna construction (TFR) or on all internal surfaces (film of carbon deposited by a methane carbonisation technique, Textor), would greatly reduce radiation losses and increase the power level causing plasma disruption. Similar results have been obtained by shaping the spectrum of the radiated spectrum (JFT2M, Mori, 1984) in order to reduce the part of the spectrum responsible for edge effects.

The near field problem is normally treated in a slab geometry (Theilhaber, 1984; Bhatnagar, 1982) solving the full wave equations in an inhomogeneous cold plasma. The good agreement with observations led the way to optimise antenna design capable of radiating waves at megawatt power levels (TFR, Equipe TFR) with high efficiency. The long pulse duration of modern large tokamaks required further development of an antenna structure capable of higher energy loading. A new antenna construction was proposed (Lallia, 1982) combining, in a simple water-cooled structure, the radiating elements and the side protection (limiter), removing the heat diffusing from the plasma.

Conceptual studies for an ICRF system for JET began in 1980 (Adam). It was proposed to choose a system with a wide frequency range (25 to 55 MHz) capable of heating the JET plasma operating at full magnetic field for either of three minority species (Hydrogen, Deuterium or Helium 3). Made of units each capable of coupling 1.5 Megawatts in the plasma, it was suggested to build the system in three successive stages. The construction of the first stage consisting of two units, started in 1982. Operation on the plasma began in 1985. The preliminary results, after the first four months of operation, are presented here. Emphasis is placed on coupling the RF waves to the plasma and on the response of the measured plasma parameters. After such a short operating period, no attempt could be made to deduce reliable confinement or heating laws and this will be the subject of a future publication.

THE JET ICRF SYSTEM

The structure of an ICRF unit is sketched in Fig. 1. Each antenna is made of two radiating elements, each connected through a long (83 - 84 m) coaxial transmission line to a 1.5 MW amplifier. Both amplifiers are driven at the same frequency and are tuned (Jacquinot, 1984) using the impedance transformation caused by a fine frequency tuning (± 0.9 MHz) and by a stub placed along the main transmission line. For most of the experiments reported here, matching was achieved with the stub located close to the generator and with a frequency kept fixed throughout the RF pulse. In some cases, a frequency feedback loop was used to trim the frequency in order to minimise the amount of power reflected to the generators. In these cases, the reflected power was below 2%; fixed frequency conditions gave normally a reflected power in the range of 5%. The two amplifiers feeding each antenna half are driven either in phase or out of phase with respect to each other. The two generator-antenna units are driven with separate oscillators and, therefore, never operate at exactly the same frequency. The amplifiers can be operated between 23 and 57 MHz in eight frequency channels, each allowing a 4 MHz bandwidth. The generators deliver the full power only if the reflected power is less than 4%. The anode voltage of the DC power supply is adjusted during the pulse in order to keep the output tetrodes in acceptable working conditions.

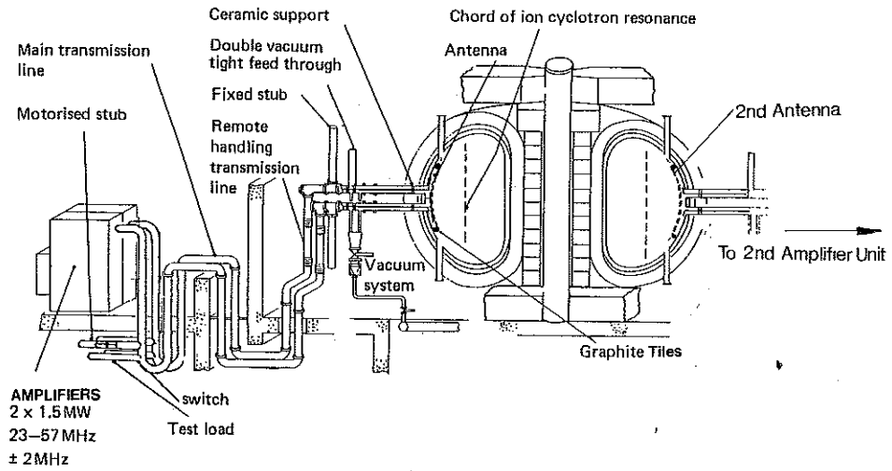

Fig. 1. Sketch of the JET ICRF system showing the organisation of an amplifier unit feeding the two halves of an antenna.

THE LAUNCHING STRUCTURE

The two antennae are installed on the low field side of the torus and at diametrically opposed toroidal locations. A frame of profiled carbon tiles protects the antenna structure from the plasma heat flux (Fig. 2). Additional thermal protection is provided by four movable carbon limiters. The radial distance between the antenna tiles and the limiters was varied from 76 mm to 6 mm. High power results have been obtained with a separation of 16 to 26 mm. In these conditions, the thermal load is shared by all six limiter structures. The antenna electrostatic screen is 17 mm behind the carbon frame. Made of nickel bars, it is designed as a wave polariser (selectively) transparent to wave electric field perpendicular to the local tokamak magnetic field. This is achieved by an inclination of the nickel bars of 15° with respect to the horizontal. The screen is responsible for some RF losses which not only can reduce the coupling efficiency but can also cause overheating. At present, the structure is not actively cooled and the pulse duration is limited to 2 sec at full power. The screen, housing and coaxial feeds of the two antennae are identical. However, they differ in the configuration of the central conductors (Fig. 3). The antenna, referred to as A_{01}, is made of two single turn coils. When the coils are fed out of phase (configuration A_{01M}, "Monopole"), the two coils reconstruct the conventional single turn normally used in ICRF experiments. In-phase feeds, however, (configuration A_{01D}, "Dipole") eliminate coupling to modes with large poloidal wave length (m = 0 modes). The antenna, referred to as A_{02}, is made of four single turn coils with internal connections producing two poloidal dipoles, separated toroidally by a distance of 20 cm and fed as previously by the two coaxial lines. Fed in phase (A_{02D}), this configuration is similar to A_{01D} but with a somewhat larger equivalent width. Feeding out of phase (A_{02Q}) in a "quadrupole mode" radiates a spectrum which is depleted for both long poloidal and toroidal wavelengths. The peak radiation occurs for a toroidal wave number of 7 m^{-1}.

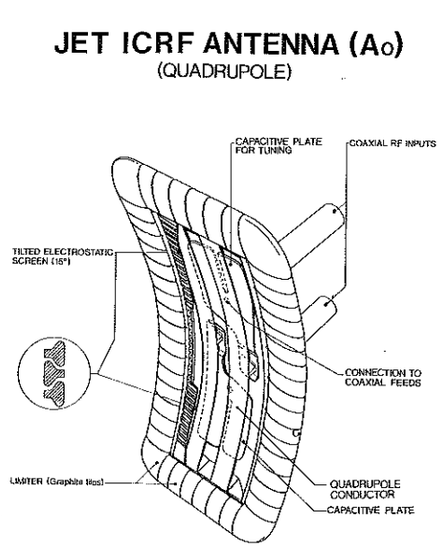

Fig. 2. Representation of an antenna showing the principal elements of the quadrupole antenna. The screen is only partly represented in order to show the internal conductors. The monopole/dipole version only differs in these conductors which are 2 single turn loops aligned in the poloidal direction.

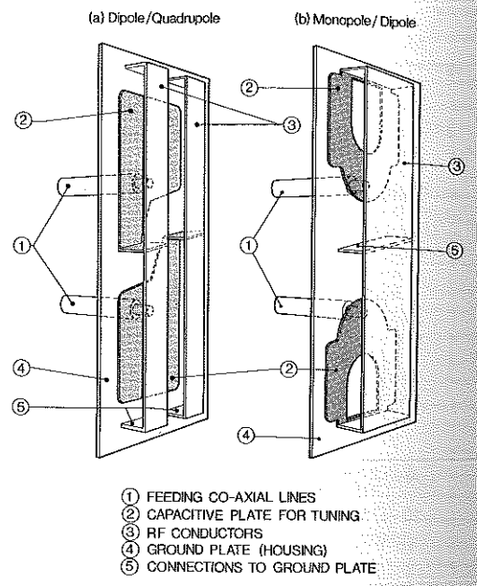

Fig. 3. Sketch of the internal RF circuits.
(a) Dipole/quadrupole case. The 4 single turn loops are connected by pairs internally. The 2 pairs can be phased to shape the $k_{//}$ spectrum in the toroidal direction.
(b) Monopole/dipole case formed of only 2 loops aligned in the poloidal direction. Π phasing gives a monopole: 0 phasing gives the dipole.

TABLE 1

Antenna	Type	Phasing between the 2 feeds	$k_{//}$ (m^{-1}) at peak radiation Toroidal	k_{θ} (m^{-1}) at peak radiation Poloidal	Maximum coupled power MW
A_{01}	Monopole	Π	0	0	2.5
	Dipole	0	0	3.5	2
A_{02}	Dipole	0	0	3.5	2.5
	Quadrupole	Π	7 m^{-1}	3.5	1.5

The characteristics of the four possible configurations are summarized in Table 1. The value of the maximum coupled power is indicative of the progress achieved to date and not of technical limitations such as voltage breakdown.

ANTENNA PLASMA COUPLING

As a figure of merit we define the antenna coupling resistance as:

$$R = 2 P Z_o^2 / V_M^2$$

Where $P = P_{inc} - P_{refl}$ is the net RF power delivered by the generator, Z_o the characteristic impedance of the line (30 Ω) and V_M the peak voltage along the feeding coaxial line. R is the resistance which, if substituted for antenna at a point of minimum impedance along the feeding coaxial line would produce the same standing wave.

The measurements of R with plasma (R_p) or without it (R_v) provide the value of the wave power effectively coupled to the Torus; this power will be referred to as P_{RF}:

$$P_{RF} = \eta P \; ; \quad \eta = \frac{R_p - R_v}{R_p}$$

Note that R_v needs to be measured in the presence of the tokamak field since one of the principal dissipative elements, the electrostatic screen, is made of nickel which can have a high magnetic permeability in the presence of carbonised or "carbidised" walls. The tokamak field completely saturates the magnetic permeability of nickel and reduces this loss.

Both antennae have R_v values in the range of 0.6 Ω at 33 MHz when matching is achieved at the generator end, 85 metres from the antenna tip. It drops to about 0.2 Ω when the matching element is located close to the antenna. Values of R_p vary widely depending on: (i) the antenna type, (ii) the distance between the plasma edge and the antenna (iii) the edge density profile. Figure 4 summarizes the coupling results. Monopole and dipole configurations have excellent coupling properties and η reaches 0.9 in most practical conditions. As expected, quadrupole phasing considerably reduces the coupling; η is only 30% (far matching) or 75% (close matching).

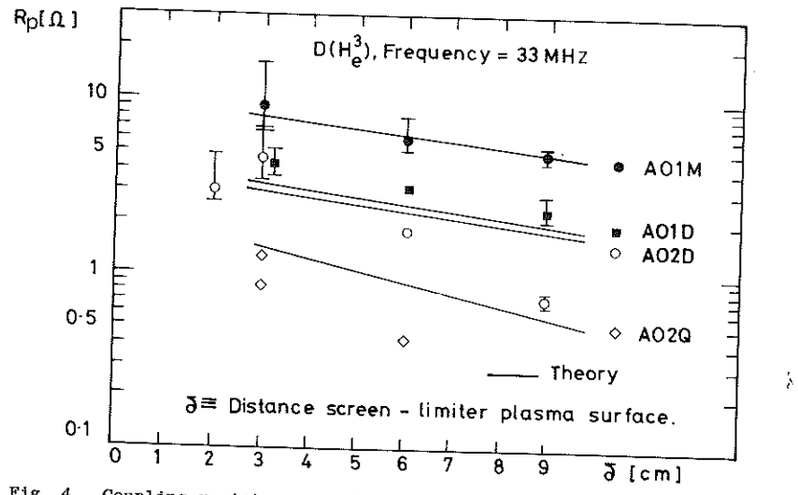

Fig. 4. Coupling resistance of the four antenna configurations. The vertical bars represent variations observed from shot to shot which are mostly related to change of plasma density. Solid lines give the values obtained from theory (Bhatnagar et al 1980).

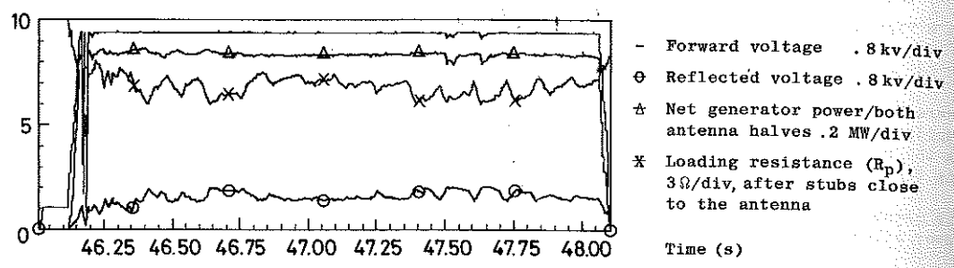

Fig. 5. Time evolution of the electrical characteristics of the quadrupole antenna. In this case short stubs close to the antenna were used to transform a loading resistance of about 0.9 Ω into 21 Ω on the generator side. The net generator power was 1.66 MW. The wave power launched in the torus was about 1.3 MW. Another example using a monopole antenna with stubs close to the antenna is shown on Fig. 6a.

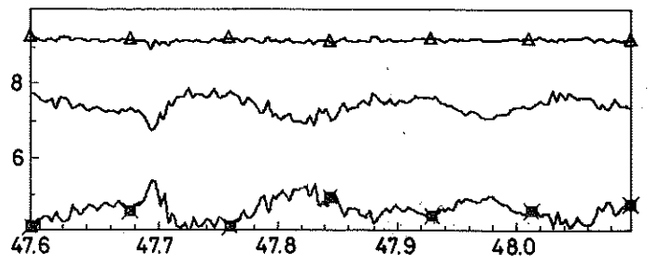

Fig. 6a Electrical characteristics of the monopole antenna during an RF pulse (2.8 MW coupled).

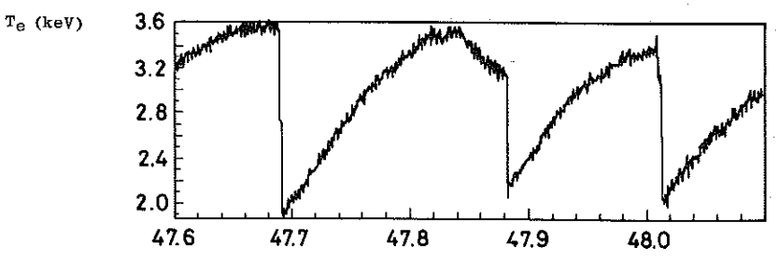

Fig. 6b Evolution of the central electron temperature (R = 3.1 m) during the same RF pulse.

Figure 5 illustrates the time evolution of the RF power signals. The coupling resistance appears fairly constant during the pulse and very similar on the two antennae halves. This maintains at low level the power reflected to the generators, without frequency tracking. In the case of significant heating in the plasma centre, the coupling resistance shows an "inverted sawteeth" behaviour in close correlation with the sawteeth relaxation of the central electron temperature (Fig. 6.). The increase of loading resistance occurs 40 ms after the internal disruption. This behaviour is compatible with a flattening of the density profile after each internal disruption. An important exception to the general behaviour mentioned is the case of the monopole which often exhibits a strong asymmetry between the coupling of the two halves. The origin of this phenomenon has not been elucidated. Preliminary comparison of these results (limited to the monopole case when behaving symetrically) to theoretical descriptions of the monopole antenna show good agreement with a model, taking into account the metallic boundary condition on each side of the antenna (Theilhaber, Jacquinot, 1984), or to a simpler 3 D model (Bhatnagar, 1982) provided the contribution to coaxial modes is excluded ($k_{//} < c/\omega$).

PLASMA HEATING RESULTS

Plasma Conditions

ICRF heating has been applied on the following target plasmas.

TABLE 2

Plasma current (MA)	2 , 2.8 , 4
Magnetic field on the axis (Tesla)	2 , 2.3 , 2.6 , 3.4
Electron line density (Deuterium is the main ion species)	6.4 10^{19} m^{-2} to 1.2.10^{20}
Z_{eff} (from Bremstralung)	∿ 3 to 5
Plasma Ellipticity	1.4 , 1.45 , 1.5
Horizontal dimension	2 m

The numbers which are underlined correspond to a consistent set of parameters (Reference condition). We will give in the following section detailed information of the response of the plasma quantities to an ICRF pulse in this particular condition which corresponds to the largest relative increase of total power (ratio 2.5) achieved, so far, with RF heating on JET. ICRF has always been operated with the vessel walls heated at 300°C and with carbonised walls, although the carbonisation could be, in some cases, fairly old (∿ 15 days). RF is normally applied 2 seconds, at least, after the beginning of the current plateau when the plasma parameters have reached a quasi steady state. The frequency is chosen in order to match, on the magnetic axis, the fundamental cyclotron resonance of the hydrogen minority (e.g. 29.8 MHz for 2 Teslas) or the Helium 3 minority (e.g. 33.2 MHz for 3.4 Teslas). The He^3 minority is injected about 2 seconds before the RF pulse and its concentration is monitored by measuring the corresponding increase of plasma electron density. The usual concentration ranges from 5 to 10% of the Deuterium density. The effect of Helium injection is quite apparent on the evolution of the antenna loading resistance, as it effectively damps the toroidal resonance in the cavity formed by the torus chamber. Cross-talk between the two antennae is also reduced by more than an order

of magnitude. Hydrogen minority heating does not normally require injection as the background hydrogen (2 to 5%) released by the limiters and the wall under plasma bombardment is sufficient to provide efficient damping.

Response of the Plasma to a Heating Pulse

Figures 7 to 10 illustrate the variation of the main plasma parameters under an ICRF heating pulse. The minority is hydrogen with n_h/n_d = 4% and the main parameters correspond to the first column of Table 2. The quadrupole antenna is first powered for 2 seconds coupling 1.3 MW into the chamber. The power on the second antenna, in the monopole mode of operation, is started 1 second later and delivers 1.5 MW for 2 seconds. During the overlapping period of 1 second, the two antennae launched a total of 2.8 MW of wave power at 29.8 MHz. This number is to be compared to a total of 3.6 MW of forward power launched by the generators. The difference results from imperfect antenna matching (∿ 0.4 MW) and from resistive losses in the antenna and transmission equipment (∿ 0.4 MW). During the same period, the ohmic power resulting from the 2 MA circulating in the plasma was quasi stationary at 1.45 MW before RF and decreased to about 1.1 MW due to the decrease of resistivity of the hotter plasma (Fig. 7a). The central electron temperature rose from 1.8 kev to about 3 kev (Fig. 8b). The volume average temperature (Fig. 9a) underwent a smaller relative increase from 0.8 to 1.1 kev. As the plasma heated up, giant sawteeth disruptions of the central electron temperature developed, reaching in some cases a temperature excursion of 1.5 kev. The temperature profile, measured with a Michelson interferometer, recording the electron cyclotron emission (Bartlett, 1983), is illustrated in Fig. 8a. The profile becomes steeper during the rise of the sawtooth. After its collapse, it takes a shape similar to the pre-RF phase. The period of the sawtooth increases with RF power. At the highest heating level achieved, the regularity of the sawteeth is broken by the appearance of sub-harmonic modulation which creates periodically super-long sawteeth reaching 250 ms, a value to be compared to 100 ms before RF is applied.

It is a common observation in JET, that the electron density rises with plasma current. This appears to be the result of desorption from the carbon limiter and carbonised wall under thermal loading. The same effect continues to apply when the thermal loading is increased as a result of additional heating. Both the line density and the central density increase at each step increase of the power (Fig. 7b). The increase saturates after about 1.5 seconds when the RF power is kept constant. Close inspection of the signal reveals that the density increase occurs in small steps following, after a short delay, an internal disruption. At the same time, a pulse of infrared light is emitted from the antenna and the limiters. It is therefore likely that the step increase of density is associated with the rapid propagation to the limiter of the heat pulse which follows an internal disruption. Multi channel interferometry shows a broadening of the density profile which is compatible with a functional form; $n_e = n_{eo}[1 - r^2/a^2]^\alpha$ with α decreasing from 0.62 to 0.55 when 2.8 MW is applied. These values are typical of freshly carbonised walls. As the carbonisation disappears, the profile becomes more peaked.

The central ion temperature is deduced from the Neutral Particle Analyser (Corti, 1983) and from the flux of neutrons produced by D-D fusion reactions (Jarvis, 1983). On both measurements some assumption has to be made, for instance, on neutral and electron density profiles. Figure 9b shows an example of deuterium temperature deduced from the neutrons. The sawteeth are also present here, although the amplitude is much smaller than with the electron temperature. There is no evidence of deviation from a Maxwellian energy distribution of the deuterium as seen from the NPA spectra and from the neutron spectrum. On the contrary, the hydrogen minority spectrum measured by the NPA shows a high energy tail. The slope of this tail corresponds to an apparent temperature of 15 keV. This tail is only observed when the wave frequency is chosen to resonate with the cyclotron frequency of hydrogen. Similar effects are expected in He^3 minority cases. They cannot be demonstrated from the NPA due to the rarity of double charge exchange of helium but can be qualitatively inferred from the observation of 14 MeV proton (Jarvis, 1983) resulting from the fusion reaction between He^3 and D.

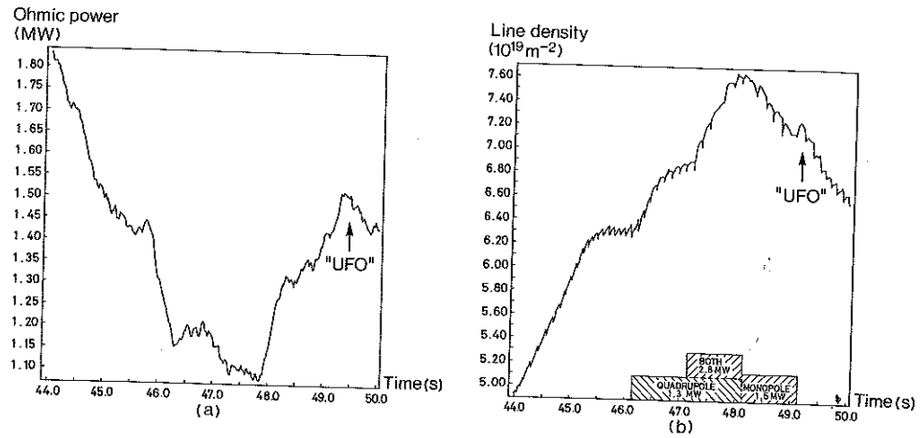

Fig. 7. (a) Evolution of the ohmic power during RF heating. The event marked "UFO", corresponds to a burst of an impurity "flying object" which was occasionally observed without correlation with RF operation. This event is also seen on Fig. 9.

(b) Evolution of the line density $n_e\ell$ along a vertical chord crossing the magnetic axis. At high density the density rise occurs in steps starting after internal disruption with a small delay of ∿ 10 ms.

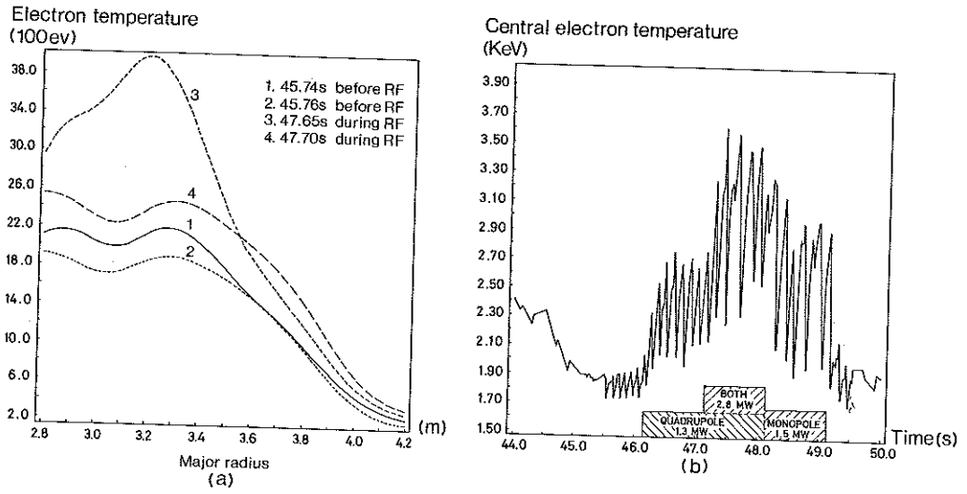

Fig. 8. Electron temperature measurements deduced from the Michelson interferometer.

(a) Temperature profiles measured at the top and at the bottom of a giant sawtooth.

(b) Evolution of the central electron temperature showing the difference of period of the giant sawteeth with the antenna type.

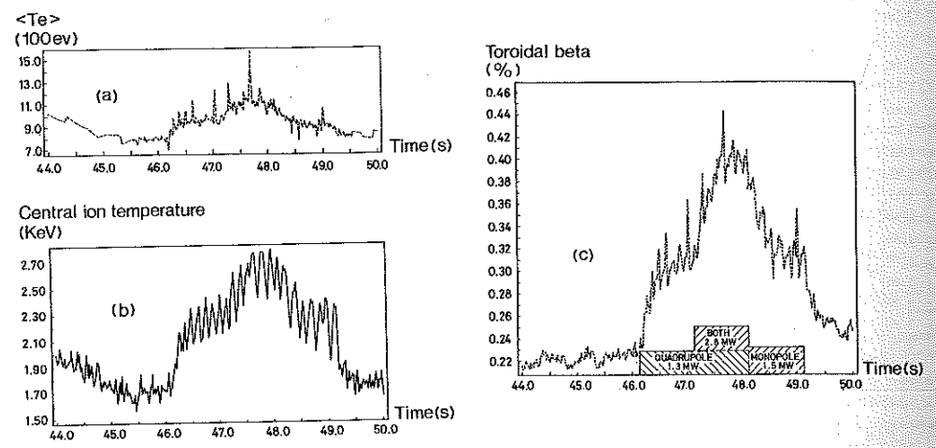

Fig. 9. (a) Evolution of the volume average electron temperature.
(b) Evolution of the central ion temperature deduced from the neutron flux and the density.
(c) Evolution of the plasma kinetic pressure normalised to the toroidal magnetic field pressure.

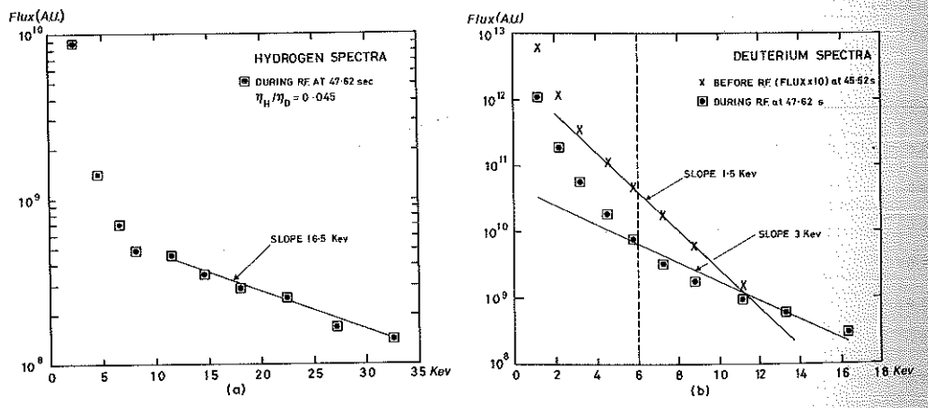

Fig. 10. Energy spectra of Hydrogen (a) and Deuterium (b) neutrals produced by charge exchange. The slopes are indicative of ions temperature in the plasma centre. When the wave frequency matches the cyclotron frequency of the Hydrogen minority, a high energy tail develops (a).

The overall effect of impurity production is measured by the evolution of the Bremstralung emission in the visible spectrum. No appreciable change can be detected when RF is applied. Bolometric measurements along several vertical and horizontal chords show that most of radiated energy is coming from the plasma periphery. The power radiated from the centre does not exceed 10% of the input power and this ratio does not appreciably change during the heating phase. The same conclusion applies to the integral of the radiated power which remains a constant or slightly decreasing fraction of the total input power. This fraction can be as low as 30% in fresh carbonisation conditions and as high as 80% when a metallic impurity influx dominates. As a general conclusion, impurity radiation never plays a significant role in the energy balance of the central part of the plasma. The radiance of metallic impurity lines such as Ni XXV or Ni XVIII increases by a factor of 2.2 for the case presented here where the total input has increased by a factor of 2,5. The level of emission saturates after 2 seconds. Peripheral lines such as C III (977 Å) rise to saturation in 0.2 seconds and also increase by a factor of 2.2. No significant differences are observed with the various phasing of the antennae in monopole, dipole or quadrupole mode. However C III radiation is smaller by a factor of 2 with the quadrupole phasing compared to both the dipole and monopole cases.

DISCUSSION AND CONCLUSIONS

The preliminary results obtained during the short initial period of operation allow us to draw the following conclusions:

a) No major difficulties were encountered with the operation of ICRF units at a level of more than 1 Megawatt and 3 Megajoules per antenna. Coupling efficiency can reach 90%.

b) The overall heating efficiency of the different types of antenna is different. Some difference can be noticed between monopole and dipole configurations, but the largest differences are found with the quadrupole which creates sawteeth of a smaller amplitude, gives a somewhat larger increase of toroidal beta (+ 20% to + 40%), increases more the edge density with a smaller carbon impurity release. It is also clear that the quantity ($d\beta/\beta dt \sim dn/ndt$) during the rise of a square RF pulse is more than a factor of 2 larger for the quadrupole case.

c) The heating power appears well localized in the centre: displacement of the heating chord on the edge of the q = 1 surface completely suppresses the enhancement of the sawtooth relaxation of the electron temperature without a significant change of stored energy.

d) Impurity effects are modest and do not play a significant role in the energy balance in the plasma centre.

e) The change of energy confinement time is similar in behaviour to results obtained by other Tokamaks in the L mode. In the example examined in detail here, the ohmic energy confinement, initially 0.5 seconds, dropped to 0.31 seconds when total input power was raised by a factor of 2.5. Nevertheless, temperatures of 3 keV have been obtained for both the electrons and the ions.

REFERENCES

Adam, J. (1975). *Plasma Physics and Controlled Nuclear Fusion Research*, I, 65.
Adam, J., J. Jacquinot, H. Kuus (1980). *EUR-CEA FC*, 1065.
Bartlett, D.V. et al. (1983). *JET Joint Undertaking Progress Report*, 86.
Bhatnagar, V.P. et al. (1982). *Plasma Physics and Controlled Nuclear Fusion Research*, IAEA, Vienna.
Corti, S. et al. (1983). *JET Joint Undertaking Progress Report*, 96.
Equipe TFR. (1980). *Plasma Physics and Controlled Nuclear Fusion Research*, IAEA, Vienna, II, 75.
Equipe TFR. (1984). *Proc. of Heating in Toroidal Plasmas*, Roma, 277.
Hosea, J. et al. (1979). *Phys. Rev. Letters*, 43.
Hwang, D.Q. et al. (1983). *Phys. Rev. Letters*, 51, 1865.
Jacquinot, J., B.D. McVey, J.E. Scharer (1977). *Phys. Rev. Letters*, 39, 88.
Jacquinot, J. (1984). *JET JDN/J/84.5*.
Jarvis, O.N. et al. (1983). *JET Joint Undertaking Progress Report*, 92.
Lallia, P.P., P-H Rebut (1982). *Heating in Toroidal Plasmas*, Grenoble, 799.
Messiaen, A. et al (1984). Private communication.
Mori, M. et al. (1984). To be published in *Proc. of the 10th Int. Conf. on Plasma Physics and Controlled Nuclear Fusion Research, London*.
Odajima, K. et al. (1984). *Proc. of Heating in Toroidal Plasmas*, Roma, 243.
Stix, T.H. and R.W. Palladino (1960). *Phys. Fluids*, 3, 641.
Theilhaber, K., J. Jacquinot (1984). *Nuclear Fusion*, Vol. 24, No. 5, 541-554.
Vdovin, V.L., V.D. Rusanov and N.V. Shapotkouskii (1976). *JETP Letters*, 24, 374.

Plasma Physics and Controlled Fusion, Vol. 27, No. 12A, pp. 1391–1398, 1985
Printed in Great Britain

0741-3335/85$3.00+ .00
Institute of Physics and Pergamon Press Ltd.

THE UK FREE ELECTRON LASER

E.W. LAING

Natural Philosophy Department, Glasgow University, Glasgow G12 8QQ, UK

(Presented at Glasgow Conference, 27 June 1985)

ABSTRACT

A brief review of the basic principles of the free electron laser is followed by a description of the UK Free Electron Laser presently being developed at the Kelvin Laboratory, Glasgow University, jointly by staff from Heriot-Watt University, Daresbury Laboratory and Glasgow University. The research programme is reviewed and future plans of the project outlined.

INTRODUCTION

A free electron laser is a device which converts the energy of a relativistic electron beam into a beam of coherent electromagnetic radiation. The basic principle of the process of conversion is the interaction of the electron beam with a modulated structure, and conventionally this structure is chosen to be a static modulated magnetic field, the Wiggler field. The effect of the Wiggler is to produce density bunching of the beam, which propagates down the beam as a longitudinal density (or electrostatic) wave. As it interacts with the Wiggler field, the density wave generates a transverse electromagnetic wave. In this brief review, the Wiggler field will be assumed to possess helical symmetry.

The combined electromagnetic field thus consists of the following:

(i) A static transverse magnetic field, axial wave number k_o (the Wiggler field).

(ii) A circularly polarized transverse electromagnetic wave parallel to the electron beam, frequency ω, wave number k_t.

(iii) A longitudinal electrostatic wave, frequency ω, wave number k_ℓ.

In the small signal limit assumed here

$$k_\ell = k_o + k_t \tag{1}$$

It can be shown that, for maximum energy transfer into the transverse electromagnetic wave, the unperturbed axial electron velocity v_{zo} must be in resonance with the phase velocity of the density wave:

$$v_{zo} = \omega/k_\ell \tag{2}$$

This condition allows an elementary derivation of the relation between ω and v_{zo}. The phase velocity of the transverse wave is close to the speed of light c, if plasma effects are negligible, that is,

$$\omega/k_t \approx c \tag{3}$$

Combining (1), (2) and (3) yields

$$v_{zo} = k_t c/(k_o+k_t)$$